

Theory and experiments of disorder-induced resonance shifts and mode edge broadening in deliberately disordered photonic crystal waveguides

Nishan Mann^{1,*}, Alisa Javadi², P.D. García², Peter Lodahl², and Stephen Hughes^{1*}

¹*Department of Physics, Queen's University, Kingston, Ontario, Canada, K7L 3N6*

²*Niels Bohr Institute, University of Copenhagen, Blegdamsvej 17, DK-2100, Copenhagen, Denmark*

(Dated: October 8, 2018)

We study both theoretically and experimentally the effects of introducing deliberate disorder in a slow-light photonic crystal waveguide on the photon density of states. We first introduce a theoretical model that includes both deliberate disorder through statistically moving the hole centres in the photonic crystal lattice and intrinsic disorder caused by manufacturing imperfections. We demonstrate a disorder-induced mean blueshift and an overall broadening of the photonic density of states for various amounts of deliberate disorder. By comparing with measurements from a GaAs photonic crystal waveguide, we find good qualitative agreement between theory and experiment which highlights the importance of carefully including local field effects for modelling high-index contrast perturbations. Our work also demonstrates the importance of using asymmetric dielectric polarizabilities for modelling positive and negative dielectric perturbations when modelling a perturbed dielectric interface in photonic crystal platforms.

PACS numbers: 42.70.Qs, 42.25.Fx, 42.82.Et, 42.81.Dp

Keywords: photonic crystal waveguides; scattering; disorder

I. INTRODUCTION

Photonic crystal (PC) cavities and waveguides are attractive nanophotonic platforms for controlling and studying fundamental light-matter interactions. Aided by the presence of a photonic band gap (PBG), which arises from the underlying periodic dielectric structure, light within a PC cavity or waveguide is strongly confined within a small volume or area. In the case of a PC waveguide (PCW), light can be slowed down by orders of magnitude compared to a typical slab or ridge waveguide, which increases the local density of photonic states (LDOS). The ability to control light-matter interactions in PC platforms leads to a host of photonic applications and rich optical interactions [1, 2]. For example, PC cavities have been used for exploring cavity quantum electrodynamics (cavity-QED) in both the weak and strong coupling regimes [3, 4], while PCWs have been exploited to realize on-chip single photon sources [5–7]. Slow-light in PCWs also enhance non-linear processes including pulse compression and soliton propagation [8], third-harmonic generation [9] and four-wave mixing [10]. In addition, PCWs have been integrated in various photonic circuits, as optical sensor elements for refractive index measurements in biosensing [11] and chemical fluid detection [12].

In practice, PCWs are highly sensitive to manufacturing imperfections (intrinsic disorder) which is inevitably introduced at the fabrication stage. Disorder-induced losses are particularly detrimental in the slow-light regime [13], which was predicted theoretically by Hughes *et al.* [14] using a photonic Green function approach and is now a common finding of various similar

theoretical works in the literature [15–18]. With continued improvements in semiconductor fabrication techniques, and improved theoretical understanding about how to mitigate disorder-induced losses [19, 20], various groups have experimentally demonstrated PCW designs that have reduced disorder-induced losses [21, 22].

However disorder in PCs is not necessarily a hindrance as was noticed by John in 1987 [23], who proposed disordered PCs for experimentally observing the well known phenomena of Anderson localization. Topolancik *et al.* [24] experimentally demonstrated spectral peaks bearing signatures of Anderson localization arising from localized modes in a deliberately disordered PCW. Patterson *et al.* [25] utilized coupled mode theory to highlight the effect of light localization via multiple scattering by examining the transmission through a PCW in the slow-light regime. The strong localized resonances in disordered PCWs have also been used to enhance the spontaneous emission factor of embedded quantum dots [26], and recently Thyrrstrup *et al.* [27] have proposed coupling quantum dot emitters to a disordered PCW as a promising platform for conducting QED experiments. Other applications of disordered PCWs include enhanced light harvesting and random lasing [28].

Apart from causing propagation losses and disorder-induced localized resonances, disorder also induces changes in the eigenfrequencies and eigenmodes of the underlying PC. Ramunno and Hughes [29] modelled disorder-induced resonance shifts in PC nanocavities and predicted a non-trivial disorder-induced mean blueshift in the cavity resonance. Patterson and Hughes [30] extended this formalism to PCWs, and predicted both a mean blueshift of resonances and a disorder-induced mode edge broadening. To the best of our knowledge, this mean blueshift has not been experimentally mea-

* nmann@physics.queensu.ca

sured; this is likely because there was no simple experimental procedure for proving that a mean blueshift occurs, especially for an intrinsically disordered PCW. Both of the theoretical works mentioned above dealt with intrinsic disorder only, which occurs via rapid fluctuations of the air-dielectric interface and highlighted the importance of carefully taking into account local fields at the interface. Recently, Savona has exploited a guided mode expansion technique to compute disorder-induced localized modes and the corresponding spectral density, which, as expected, showed sharp spectral signatures near the mode edge indicative of spatially localized modes [31].

In this paper, we introduce a model to describe disorder-induced resonance shifts and broadening of the fundamental mode near the mode-edge which takes into account a systematic increase of the disorder parameters (i.e., it allows one to model deliberate disorder which can be controlled and changed in a systematic way). This leads to a predictable trend that causes an increasing mean blue shift and a broadening of the photonic density of states (DOS). We show how one can extend the theoretical models introduced in Refs. [29, 30] to account for both intrinsic and deliberate or extrinsic disorder where extrinsic disorder is characterized by a deliberate shift of the hole centres. We carefully include local field effects [32] in our model to compute the first and second-order perturbative changes to the eigenfrequencies of the fundamental waveguide mode which then allow us to compute the disordered DOS. For disordered PCWs with varying extrinsic disorder (see Ref. [33] for details), we compute the ensemble averaged DOS via a Monte Carlo approach. Experimentally, measurements of vertically emitted intensity are taken for GaAs PCW membranes with varying amounts of extrinsic disorder. Since the intensity measurements are a direct measure of disordered-induced broadening and frequency shift (blueshift) of the DOS, we compare our computed DOS with the intensity measurements and the two are found to be in good qualitative agreement. The comparison between our theory and experimental data demonstrates the importance of including local field effects when computing disorder-induced changes to the eigenfrequencies and eigenmodes of PCWs. While our theory is perturbative, the semi-analytical approach is computationally efficient and the results offer useful insights in designing disordered PCWs for spontaneous emission enhancements of embedded quantum dots. Finally, we also show an example of the underlying disorder-induced quasimodes that can be obtained on a finite-size PC lattice by computing the numerically exact Green function using a full 3D FDTD approach [6].

Our paper is organized as follows. In Section II we review our formalism for modelling disorder-induced resonance shifts and point out the limitations of some of the polarization models commonly used in literature for modelling disorder in PCWs. We then introduce our extended polarization model for modelling both intrinsic

and extrinsic disorder and show how it results in a non-vanishing first-order frequency shift. In Section III, we highlight our approach for computing the disordered DOS given disorder-induced resonance shifts. We also present a mathematical argument based on photonic Green functions that link the disordered DOS to vertically emitted intensity measurements. In Section IV, we numerically compute disorder-induced resonance shifts and the disordered DOS which we compare with experimental measurements performed on GaAs PCW membranes. While we find qualitatively good behaviour, in Section V we discuss some limitations of our perturbative model and we also show some numerically exact simulations of finite-size PCWs, which are limited in spatial size because of the numerical complexities. In Section VI, we summarize the strengths and weaknesses of our perturbative semi-analytical approach and discuss our results in the context of previous reports in the literature. We conclude in Section VII.

II. DISORDER-INDUCED RESONANCE SHIFTS AND DISORDER POLARIZATION MODELS

For modelling the effects of disorder on light scattering in PCWs, we focus our attention on deriving the first and second order perturbative changes to the eigenfrequencies of a dielectric structure. We treat disorder as a perturbation and employ perturbation theory techniques adapted to dielectric structures with high index contrasts [32, 34]. Denoting the perturbed eigenfrequencies as $\omega = \omega_0 + \sum_i \Delta\omega^{(i)}$, where ω_0 is the unperturbed eigenfrequency and $\Delta\omega^{(i)}$ represents the i^{th} order perturbation, we restrict ourselves to the first $\Delta\omega^{(1)}$ and second order $\Delta\omega^{(2)}$ corrections. Since disorder in PCWs is statistical in nature, we compute the ensemble average over nominally identical disordered PCWs denoted by $\mathbb{E}[\]$. Thus the first-order ensemble averaged correction is given by [29] (ω dependence is implicit)

$$\mathbb{E}[\Delta\omega^{(1)}] = -\frac{\omega_0}{2} \int_{\text{cell}} \mathbb{E}[\mathbf{E}^*(\mathbf{r}) \cdot \mathbf{P}(\mathbf{r})] d\mathbf{r}, \quad (1)$$

where $\mathbf{E}(\mathbf{r})$ is the unperturbed eigenmode, $\mathbf{P}(\mathbf{r})$ is the polarization function to characterize the dielectric disorder, and the integration is carried out over the primitive unit cell of the PC lattice. The fields are normalized according to $\int_{\text{cell}} \varepsilon(\mathbf{r}) \mathbf{E}^*(\mathbf{r}) \cdot \mathbf{E}(\mathbf{r}) d\mathbf{r} = 1$, where $\varepsilon(\mathbf{r})$ is the unperturbed dielectric constant. The ensemble average of the second-order correction $\mathbb{E}[\Delta\omega^{(2)}]$, is computed similarly [30]

$$\mathbb{E}[\Delta\omega^{(2)}] = \frac{\omega_0^2}{4} \iint \mathbb{E}[\mathbf{E}^*(\mathbf{r}) \cdot \mathbf{P}(\mathbf{r}) \mathbf{E}^*(\mathbf{r}') \cdot \mathbf{P}(\mathbf{r}')] d\mathbf{r} d\mathbf{r}'. \quad (2)$$

To interpret the ensemble averages of the first and second order corrections in a statistical sense, we de-

note the *net frequency shift* as $\Delta\omega (\sum_i \Delta\omega^{(i)})$, with $\omega = \omega_0 + \Delta\omega$. The net frequency shift $\Delta\omega$ is interpreted as a random variable whose probability distribution has $\mathbb{E}[\Delta\omega^{(1)}]$, $\mathbb{E}[\Delta\omega^{(2)}]$ as its first and second-order moments, respectively. Hence, given the unperturbed eigenmodes, one is left with choosing a suitable polarization model to describe the perturbation of the PC lattice. Structural disorder in PCWs can be viewed as introducing additional scattering sites in an otherwise perfect PCW lattice. The scattering sites induce dipole moments resulting in a disorder-induced polarization which acts as a source term in the homogeneous Maxwell equations, thus contributing to scattering of a propagating Bloch mode. An alternative picture is that perturbations will disorder the PC band structure and thus the DOS, which will result in disorder-induced localization modes and scattering in directions that might otherwise be forbidden (e.g., a lossless propagating mode will couple to radiation modes above the light line in the case of a PCW slab).

There are typically two models that have been widely used in the photonics community for modelling dielectric perturbations, which denote as *weak-index contrast* $\mathbf{P}_w(\mathbf{r})$ and *smooth-perturbation* $\mathbf{P}_s(\mathbf{r})$. The former model neglects the problem of field-discontinuities at high-index-contrast surfaces, and is well defined for field components that are parallel to the interface; in contrast, the latter model addresses this field-discontinuity problem, though it is appropriate for perturbing a surface uniformly in a perpendicular direction, e.g., displacing a long sidewall in a direction that is perpendicular to the wall interface. By way of a simple example, consider a simple planar interface between two dielectrics ε_a , ε_s , located at \mathbf{r}' . When perturbed by a small amplitude Δh , the two polarization models are given as:

$$\mathbf{P}_w(\mathbf{r}) = \Delta\varepsilon\Delta h(\mathbf{r})\mathbf{E}(\mathbf{r})\delta(\mathbf{r} - \mathbf{r}'), \quad (3)$$

$$\mathbf{P}_s(\mathbf{r}) = \Delta\varepsilon\Delta h(\mathbf{r}) \left(\mathbf{E}_{\parallel}(\mathbf{r}) + \frac{\varepsilon(\mathbf{r})}{\varepsilon_a\varepsilon_s} \mathbf{D}_{\perp}(\mathbf{r}) \right) \delta(\mathbf{r} - \mathbf{r}'), \quad (4)$$

where $\Delta\varepsilon = \varepsilon_a - \varepsilon_s$ or $\Delta\varepsilon = \varepsilon_s - \varepsilon_a$ depending on the direction of the perturbation, i.e. from ε_a to ε_s or vice versa, and $\mathbf{E}_{\parallel}(\mathbf{r})$, $\mathbf{D}_{\perp}(\mathbf{r})$ denote the parallel and perpendicular components of the electromagnetic fields relative to the boundary interface. The weak-index contrast model is accurate in systems exhibiting weak-index contrast (i.e., $|\Delta\varepsilon| \ll 1$) and is the most popular choice for modelling imperfections in dielectric structures such as optical waveguides [35]. In high-index contrast systems such as PCWs, the quantity $\Delta\varepsilon|\mathbf{E}|^2$ is, however, generally ill-defined at the interface due to a large step discontinuity in \mathbf{E}_{\perp} [34], hence the smooth-perturbation model is likely more appropriate at the interface due to the use of continuous field components. The smooth-perturbation model is expected to be valid as long as the perturbation is smooth. Both models have been used to compute disorder-induced losses in PCWs [14, 16, 30, 36] and have yielded a good qualitative understanding of the observed disorder-induced loss phenomena.

If one views the perturbation (smooth or piecewise smooth) as introducing scatterers into the system, one must take into account their respective polarizabilities which in general depend on the direction of the perturbation. The weak-index contrast and smooth-perturbation models assign polarizabilities that differ only in sign when the direction of perturbation is reversed but remain unchanged in magnitude. Moreover, the magnitude of the polarizability of a scatterer can be drastically different in the weak-index approximation as demonstrated by the example of a small dielectric sphere in a homogeneous background (see Ref. [37]). Therefore, in general for piecewise smooth perturbations such as bumps on an interface, it is important to compute polarizabilities that correctly take into account the direction of perturbation. To address this concern, Johnson *et al.* [32] introduced the *bump-perturbation* polarization model, denoted by $\mathbf{P}_b(\mathbf{r})$ to model surface roughness in PCWs as piecewise smooth bumps on the interface, where

$$\mathbf{P}_b(\mathbf{r}) = [\varepsilon_{\text{avg}}\alpha_{\parallel}\mathbf{E}_{\parallel}(\mathbf{r}) + \varepsilon(\mathbf{r})\gamma_{\perp}\mathbf{D}_{\perp}(\mathbf{r})] \Delta V\delta(\mathbf{r} - \mathbf{r}'), \quad (5)$$

where $\varepsilon_{\text{avg}} = \left(\frac{\varepsilon_a + \varepsilon_s}{2}\right)$, and α_{\parallel} , γ_{\perp} denote the polarizabilities (polarizability tensors per unit volume) of the bump perturbation and ΔV is the volume of the disorder bump element. This model is valid for arbitrary dielectric contrasts and bump shapes, and useful formulas have been obtained for rectangular and cylindrical shaped bumps [32]. Using the polarizabilities for a cylindrical bump shape, this model has been used to model resonance shifts caused by intrinsic disorder in PCWs [30] where a mean blueshift and broadening of the ideal bandstructure was found. As was noted in Ref. [30], resonance shifts in the band structure are not predicted by either the weak-index contrast or the smooth-perturbation models.

In this work, we apply the *bump-perturbation* model with cylindrical bump shape polarizabilities, to compute disorder-induced resonance shifts in PCWs, and systematically investigate what happens with an increase in the disorder parameters for shifted holes. We use this model to connect to related experiments on deliberately disordered GaAs membranes where embedded quantum dots couple to disorder-induced localized modes resulting in enhanced spontaneous emission [26, 33]. The PCW we consider is a standard W1 formed by introducing a line defect in a triangular lattice of air holes etched in a semiconductor slab Fig. 1(a). The extrinsic disorder perturbation is characterized by a hole centre shift as shown in Fig 1(b). The air holes are cylinders so we employ cylindrical coordinates (r, θ, z) henceforth. Furthermore, the disordered air hole is assumed to have a constant cross section throughout the slab thickness. This allows us to replace the disorder volume element in Eq. (5) by its cross-sectional area ΔA and the polarizabilities are now 2×2 tensors representing polarizability per unit area [32]. To first order, the perturbed area ΔA of the disorder element is proportional to $|\Delta h|$ which quantifies the amplitude of the hole centre shift.

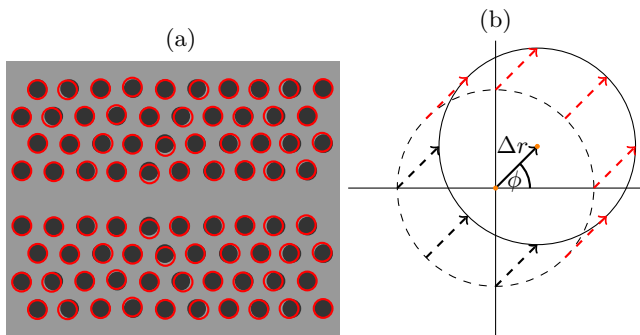


FIG. 1. (Color Online) (a) Schematic of a disordered WI with ideal air holes (dark-filled/black circles), disordered holes (light/red circles) and the background slab (grey). (b) Schematic of a hole centre shift with the centres marked by light-filled/orange circles and the direction of perturbation given by the solid-black arrow. The magnitude of the perturbation is denoted by Δr and the direction is given by ϕ . Dashed arrows indicate the shifts of the air-slab interface with dashed-red/light and dashed-black/dark arrows representing positive and negative shifts respectively.

In light of current experiments studying localization modes and resonance shifts as a function of deliberate disorder, we extend the disorder model of Ref. 30 to deal with both intrinsic and varying extrinsic disorder. While the previous model considered rapid radial fluctuations of the air-slab interface as the source of intrinsic disorder, here we model both intrinsic and extrinsic disorder as a net centre shift of the air hole as shown schematically in Fig. 1(b). Although intrinsic disorder is likely best described by rapid radial fluctuations, the choice to model intrinsic disorder as a hole centre shift is driven by simplicity as one can map rapid radial fluctuations to an effective hole centre shift by comparing experimental loss data with numerical simulations as demonstrated by Garcia *et al.* [38]; also, the main effect of the disorder below is through deliberate disorder.

Since disorder is stochastic in nature, we denote $(\Delta h, \phi)$ as the random variables quantifying the total disorder (extrinsic and intrinsic) in PCWs. The net amplitude of the shift $|\Delta h|$ is constant around the circumference while the sign is determined by the net azimuthal direction of the shift, denoted by ϕ . The shift of an infinitesimally small arc lying on the circular air-slab interface is then given by

$$\Delta h(\Delta r, \phi; \theta) = \begin{cases} +\Delta r, & \phi \in \Omega, \\ -\Delta r, & \phi \notin \Omega, \end{cases} \quad (6)$$

where $\Omega = [\theta - \frac{\pi}{2}, \theta + \frac{\pi}{2}]$, θ denotes the polar coordinate and Δr quantifies the net radial perturbation. A positive bump/shift ($+\Delta r$) is defined as the air-slab boundary shifting into the slab and vice versa for negative bumps/shifts as illustrated in Fig. 1(b). We denote $\Delta r_{i/e} \sim |\mathcal{N}(0, \sigma_{i/e})|$, $\phi_{i/e} \sim \mathcal{U}[-\pi, \pi]$ as the random variables for the radial magnitudes and azimuthal directions

of the intrinsic/extrinsic disorder perturbations, respectively; $\mathcal{N}(\mu, \sigma)$ denotes a normal distribution with mean μ and standard deviation σ while $\mathcal{U}[a, b]$ denotes a uniform distribution on the interval $[a, b]$. The net radial fluctuation can be broken down into its Cartesian components Δx , Δy , which are given below

$$\Delta x = \Delta r_i \cos(\phi_i) + \Delta r_e \cos(\phi_e), \quad (7)$$

$$\Delta y = \Delta r_i \sin(\phi_i) + \Delta r_e \sin(\phi_e). \quad (8)$$

The net radial fluctuation is then given as $\Delta r = \sqrt{\Delta x^2 + \Delta y^2}$ while the net azimuthal direction is simply $\phi = \tan^{-1} \left(\frac{\Delta y}{\Delta x} \right)$. Comparing to our previous model of rapid radial fluctuations [30], this model lacks the concept of an intra-hole correlation length as all points on the hole shift by the same magnitude but in different directions depending on the angular hole coordinate θ . However this model is more appropriate for modelling the deliberate displacement of the disordered holes performed in the experiment.

To highlight the main difference between the three polarization models discussed earlier, let us look at computing the ensemble averaged first-order frequency shift $\mathbb{E}[\Delta\omega^{(1)}]$ by using Eqs. (3), (4) or (5) in Eq. (1). For weak-index contrast and smooth-perturbation models, one must compute the expectation of the total disorder $\mathbb{E}[\Delta h]$. If the extrinsic disorder is zero ($\sigma_e = 0$), it is trivial to show that $\mathbb{E}[\Delta h] = 0 \rightarrow \mathbb{E}[\Delta\omega^{(1)}] = 0$. In the case where both intrinsic and extrinsic disorder are present, one can still show $\mathbb{E}[\Delta h] = 0$ as can be verified via a Monte Carlo simulation. This result is expected because given any random value for the net radial displacement Δr , all possible azimuthal directions are equally likely; and since we are assigning symmetric weights (differing only in sign) to positive and negative shifts in these two models, the first order correction vanishes. This is in line with previous findings where intrinsic disorder was modelled as rapid radial fluctuations [30]. However, a non-zero first-order mean frequency shift is expected to occur for the bump-perturbation model since $\mathbb{E}[\alpha_{\parallel} \Delta h] \neq 0$, $\mathbb{E}[\gamma_{\perp} \Delta h] \neq 0$. This is because the polarizabilities for the shifts that we use in Eq. (5) are *asymmetric*, i.e. $\alpha_{\parallel}^+ \neq \alpha_{\parallel}^-$, $\gamma_{\perp}^+ \neq \gamma_{\perp}^-$ where $+/-$ denote positive and negative shifts respectively. For the second order correction $\mathbb{E}[\Delta\omega^{(2)}]$, none of the expectation terms vanish and therefore the variance of the net mean frequency shift is non zero for all three polarizability models. One way to test which model is more appropriate is to compare with experiments where the amount of disorder can be controlled, and that is precisely what we do below.

III. DISORDERED DENSITY OF STATES AND CONNECTION TO EXPERIMENTS OF VERTICAL LIGHT EMISSION

Since disorder acts to shift and broaden the mode edge, a useful quantity for experimental comparison is the DOS

$\rho(\omega(\mathbf{k}))$, defined as the number of frequency levels per unit volume of \mathbf{k} -space. Unlike the concept of bandstructure, which is only well-defined in perfectly periodic systems, the DOS is valid for all structures. It is well known that the DOS of an ideal PCW diverges at the mode edge since the group velocity vanishes, while for a disorder PC structure, the ensemble averaged DOS exhibits a broadened peak around the ideal mode edge where the width of the peak is proportional to the amount of disorder present in the PC structure [39].

To compute the DOS, we first remark that the definition of DOS bears close resemblance to the mathematical definition of a probability density function (PDF). Hence, just like a histogram generated from a large sample dataset represents the underlying PDF, the histogram generated from a bandstructure represents the DOS. To generate a disordered DOS instance, we generate a disordered bandstructure given by $\omega(k) = \omega_0(k) + \Delta\omega(k)$ where the net frequency shift $\Delta\omega(k)$ is a random variable *assumed* to have a normal distribution with mean $\mathbb{E}[\Delta\omega^{(1)}(k)]$ and variance $\mathbb{E}[\Delta\omega^{(2)}(k)]$. The disordered bandstructure allows us to calculate an instance of the disordered DOS $\rho(\omega)$. One then computes the ensemble averaged disordered DOS $\bar{\rho}(\omega)$ by averaging over many such disordered DOS instances.

Experimentally, the DOS can be obtained by spatially averaging the vertically emitted light intensity measurements in PCWs. To appreciate how the waveguide DOS can be measured through vertical emission, consider the waveguide mode Green function without any disorder [40]:

$$\mathbf{G}_{\text{wg}}(\mathbf{r}, \mathbf{r}'; \omega) = \frac{ia\omega}{2v_g} [\Theta(x - x') \mathbf{f}_k(\mathbf{r}) \mathbf{f}_k^*(\mathbf{r}') e^{ik(x-x')} + \Theta(x - x') \mathbf{f}_k^*(\mathbf{r}') \mathbf{f}_k(\mathbf{r}) e^{-ik(x-x')}], \quad (9)$$

where $\Theta(x - x')$ is the Heaviside function, $k = k(\omega)$ and \mathbf{f}_k is the ideal Bloch mode. Now consider adding a point disorder model, where the disorder causes a polarizability with a Lorentzian lineshape (e.g., typical of a disorder-induced resonance or an embedded light source such as a quantum dot), $\alpha^d = A/(\omega_0 - \omega - i\gamma)$, where ω_0 is the disorder induced resonance frequency, γ is the broadening of the resonance, and A is the coupling strength. Using a Dyson equation, $\tilde{\mathbf{G}} = \mathbf{G} + \mathbf{G}\alpha^d\tilde{\mathbf{G}}$, the Green function in the presence of the perturbation can be exactly obtained through $\tilde{\mathbf{G}}$, where α^d has units of volume (polarizability volume) and the Green function has units of inverse volume. Defining $\rho_i(\mathbf{r}_d) \equiv \text{Im}[\mathbf{G}_{ii}(\mathbf{r}_d, \mathbf{r}_d)]$ where $\text{Im}[\]$ denotes the imaginary component as a measure of the (projected) LDOS, we obtain

$$\tilde{\rho}_i(\mathbf{r}_d, \omega) = \rho_i(\mathbf{r}_d, \omega) \frac{(\omega - \omega_0)^2 + \gamma[\gamma + A\rho_i(\mathbf{r}_d, \omega)]}{(\omega - \omega_0)^2 + [\gamma + A\rho_i(\mathbf{r}_d, \omega)]^2}, \quad (10)$$

and thus the disordered LDOS now contains signatures of the original waveguide LDOS and the underlying res-

onance of the disorder site. Looking at the limit $\omega \rightarrow \omega_0$,

$$\tilde{\rho}_i(\mathbf{r}_d, \omega_0) = \rho_i(\mathbf{r}_d, \omega_0) \frac{\gamma}{\gamma + A\rho_i(\mathbf{r}_d, \omega_0)}, \quad (11)$$

where we note that the LDOS at the mode edge is no longer divergent, and instead $\tilde{\rho}_i(\mathbf{r}_d, \omega_e) = \gamma/A$ (assuming $\omega_0 = \omega_e$), which is simply the LDOS from the disordered polarizability model. Since this disordered LDOS is now connected to light propagation away from the waveguide, vertically emitted light will clearly contain signatures of the disordered LDOS for the waveguide modes, and thus the disordered DOS when spatially integrated.

An alternative picture of the disordered DOS can be obtained by connecting directly to a sum over the disordered-induced modes. In PCWs, propagating and localized modes couple with radiation modes above the light line resulting in vertically emitted intensity. Near the mode edge, the DOS increases due to vanishing group velocity leading to an increase in the radiation loss rate and a broadened peak in the vertically emitted intensity spectrum. Other peaks in the spectrum near the mode edge indicate the presence of disorder-induced localized modes. Given that the vertically emitted intensity is proportional to the radiation loss rate, denoted by γ , one can show that the radiation loss rate is proportional to the DOS. Let us assume the disordered quasimodes (or quasinormal modes) [42] are known or can be computed, denoted by $\tilde{\mathbf{f}}_j(\mathbf{r})$ where j indexes the quasimodes which have complex eigenfrequencies $\tilde{\omega}_j = \omega_j + i\gamma_j$, where the quality factor of each resonance is $Q_j = \omega_j/2\gamma_j$. Then using mode expansion, one obtains the Green function of the disordered PCW by [43, 44]

$$\mathbf{G}_{\text{dis}}(\mathbf{r}, \mathbf{r}'; \omega) = \sum_j \frac{\omega^2}{2\tilde{\omega}_j(\tilde{\omega} - \omega)} \tilde{\mathbf{f}}_j(\mathbf{r}) \tilde{\mathbf{f}}_j^*(\mathbf{r}'), \quad (12)$$

and the LDOS of the disordered PCW is

$$\rho(\mathbf{r}, \omega) = \frac{2}{\pi\omega} \text{Im}[\text{Tr}\{\mathbf{G}_{\text{dis}}(\mathbf{r}, \mathbf{r}; \omega)\}], \quad (13)$$

where $\text{Tr}[\]$ denotes the trace. From the total LDOS one can compute the DOS by integrating over all space. Therefore one sees that the radiation loss rate and the vertically emitted intensity is inherently linked to the disordered DOS. Indeed, each one of the underlying quasimodes (and every disordered element) has a vertical decay channel associated with vertical decay above the light line.

IV. CALCULATIONS AND MEASUREMENTS OF THE DISORDERED-INDUCED RESONANCE SHIFTS AND DENSITY OF STATES

The experimental samples are W1 GaAs membranes with a pitch of $a = 240$ nm and thickness 150 nm with an embedded layer of InAs self-assembled quantum dots at the centre of the membrane having uniform density

of $80\mu\text{m}^{-2}$. Quantum dots present a very similar refractive index to that of the surrounding membrane material (GaAs). In addition, the experiments presented in this paper are carried out under high excitation power ($57\mu\text{W m}^{-2}$) [33], which drives the quantum dots beyond saturation, and they become transparent. For these reasons, we consider negligible quantum dot contribution to both inelastic and elastic scattering and, thus, we can rule out any quantum dot contribution to our model. Various samples each measuring $100\mu\text{m}$ long are manufactured with varying degrees of extrinsic disorder. Extrinsic disorder is introduced via an additional hole centre displacement characterized by σ_e and is varied from $0.01a = 2.4\text{ nm}$ to $0.05a = 12\text{ nm}$ in $0.01a = 2.4\text{ nm}$ steps. The samples are excited and vertically emitted intensity is collected as function of wavelength and position along the waveguide direction $I(\lambda, x)$ as shown in Figs. 3(a,b). The intensity is then spatially integrated along the waveguide $I(\lambda) = \int I dx$ as shown in Fig. 3(c).

To connect to these experiments, we model a corresponding W1 PCW (see Fig. 1(a)) with a slab dielectric constant suitable for GaAs ($\epsilon = 12.11$), with the following parameters: $r = 0.295a$ (hole radius), $h = 0.625a$ (slab height). The ideal bandstructure (i.e., with no disorder) is plotted in Fig. 2(a), depicting the fundamental lossless guided mode that spans from 876 nm (thereafter going above the light line) to 930 nm (mode edge). The intrinsic disorder is approximated as an effective hole centre of shift (see Ref. [38]), and is kept fixed at $\sigma_i = 0.005a = 1.2\text{ nm}$.

The ensemble averaged first and second-order frequency corrections assuming the bump-perturbation model for all samples are plotted in Figs. 2(c), (d). The expectations in Eqs. (1,2) were computed numerically, that is given the statistical parameters for disorder, N samples of the set $(\Delta r_i, \Delta r_e, \phi_i, \phi_e)$ are drawn from the underlying probability distributions which yields $N = 10^4$ samples of Δh . The integration is carried out via Riemann sums where the step size is chosen to be small enough (3 nm) to ensure numerical convergence.

Interpreting the first and second order frequency corrections as the mean and variance of the net frequency shift (see Sec. II), from Fig. 2(c,d), we see that for all cases of disorder, the mean frequency shift is a *blueshift* with a standard deviation that increases as the total amount of disorder increases. We note that the prediction of a mean blueshift is non-trivial and is solely due to the asymmetric polarizabilities present in bump-perturbation polarization model. Since one is often concerned with the mode-edge or cutoff of the fundamental guided mode in PCWs, we find that the mode-edge mean shift and variance is roughly of the same order as the amount of disorder in the system. For example, for extrinsic disorder of $0.02a(4.8\text{ nm})$, the mode edge is blueshifted roughly by 4 nm with a standard deviation of approximately 4 nm . From a bandstructure point of view, the mean frequency shift and variance act to shift and broaden the bandstructure as shown in Fig. 2(b) for

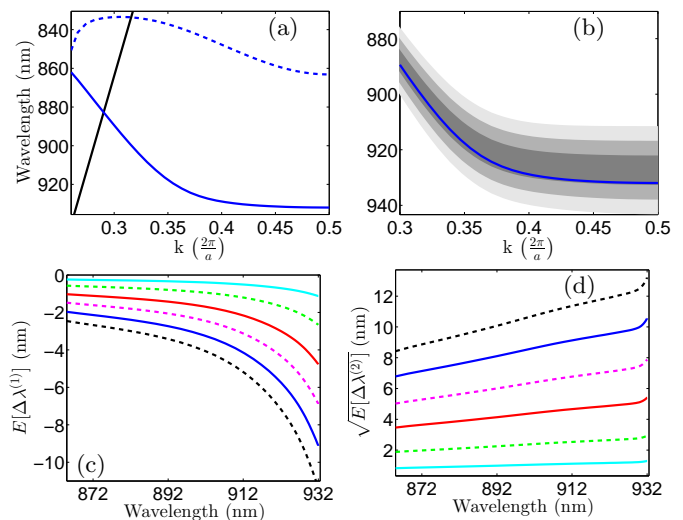


FIG. 2. (Color online) (a) Photonic bandstructure (in units of wave vector versus vacuum wavelength) of the ideal W1 showing the fundamental (solid) and higher order (dashed) guided modes. The light line is shown in black. (b) The broadened (blueshifted on average) bandstructure of the unperturbed fundamental mode (blue/dark-solid line) for extrinsic disorder of $0.02a(4.8\text{ nm})$. The three greyscale shades indicate the statistical distribution of the perturbed eigenfrequencies that lie within $\pm\sigma$, $\pm2\sigma$, $\pm3\sigma$ (dark-grey, medium-grey, light-grey) of the unperturbed fundamental mode, where σ denotes the standard deviation. (c) Ensemble averaged first-order eigenvalue corrections for six disordered samples representing the mean net frequency shift. (d) Ensemble averaged second-order eigenvalue corrections representing the standard deviation of the mean net frequency shift. In both graphs, the *intrinsic* disorder is kept fixed at $0.005a(1.2\text{ nm})$ while the external disorder is varied as follows: $0a$ (cyan/solid-light-grey), $0.01a(2.4\text{ nm})$ (green/dashed-light-grey), $0.02a(4.8\text{ nm})$ (red/solid-medium-grey), $0.03a(7.2\text{ nm})$ (magenta/dashed-medium-grey), $0.04a(9.6\text{ nm})$ (blue/solid-dark-grey), $0.05a(12\text{ nm})$ (dashed-black).

the case with $0.02a(4.8\text{ nm})$ of extrinsic disorder. The three grayscale shades demonstrate the statistical nature of the frequency shift by differentiating between frequencies that lie within $\omega_0 \pm \sigma$, $\omega_0 \pm 2\sigma$, $\omega_0 \pm 3\sigma$ where σ denotes the standard deviation and ω_0 is the unperturbed frequency.

The normalized experimental intensity spectra for two different amounts of extrinsic disorder along the waveguide is shown in Figs. 3(a,b). Integrating along the waveguide direction, the corresponding intensity spectra is compared to the ensemble averaged disordered DOS for the six samples (considered previously in Fig. 2) in Figs. 3(c,d). For now we neglect the contribution of radiation modes to the DOS which scales roughly as $1/\lambda^2$ (Please see Fig. 3(c) for how this might look like). Treating the DOS as a probability distribution as mentioned in Sec. III, each DOS instance histogram had a sample size of 1000 (number of k-points) and bin resolution of 0.27 nm (200 bins). The ensemble-averaged disordered

DOS was calculated from 500 DOS instances. Note, as discussed earlier, the DOS at the mode edge formally diverges (as the group velocity approaches zero) in the absence of disorder but our computed disordered DOS is non divergent and shows a pronounced mean blueshift as well as broadening caused by the variance of the net frequency shift. This agrees qualitatively well with the experimental intensity spectra except for the cases of high extrinsic disorder $\sigma_e = 0.05a$ (12 nm) where the theory overestimates the broadening and for $\sigma_e = 0.02a$ (4.8 nm); where the theory predicts a blueshift, but the experimental intensity spectra is redshifted. The observed redshift of the mode-edge is within the computed variance so it is either that this discrepancy arises due to the experimental sample representing only one disorder instance or the fabrication method of these particular waveguides where a, e.g., proximity effect could introduce an additional unknown degree of disorder different from the designed one.

We now discuss some limitations to our perturbative approach. For extrinsic disorder values greater than or equal to $0.04a$ (9.6 nm), the computed DOS is too broad when compared to the measured intensity, see Fig. 3(c),(d). This broadening results from the increase in standard deviation of mean frequency shift as shown in Fig. 2(d). Strictly speaking, our perturbation theory computes mode edge resonance shifts and broadening for *periodically* disordered PCWs; that is the primitive unit cell is disordered and then repeated indefinitely. This is an approximation as in reality the disordered PCW is a concatenation of disordered unit cell instances sampled from an underlying probability distribution. Moreover for the extreme extrinsic disorder case of $0.05a$ (12 nm), we can see the signature of new localized mode forming below the mode edge around 945 nm in the intensity spectrum (Fig. 3(c)) which our computed DOS cannot reproduce since localized modes that form due to cavity-like defects are naturally not present in a waveguide exhibiting periodic disorder.

To assess the role of multiple scattering qualitatively, we considered incoherent disorder-induced losses in our samples, with and without multiple scattering. With the mode edge roughly corresponding to a group index of $n_g \approx 50$, our computations indicate that for $n_g > 20$, we are already in the regime of multiple scattering for all amounts of disorder. Therefore, akin to the overestimation of losses without multiple scattering [45], the *periodic* disorder perturbative approach provides an upper bound for mode edge broadening and for more realistic predictions, a nonperturbative approach is needed that takes into account multiple scattering effects. Such an approach is very numerically demanding and is beyond the scope of this first paper on the topic. However, below we show some numerically exact solutions of disorder-induced resonances and LDOS for short length PCWs.

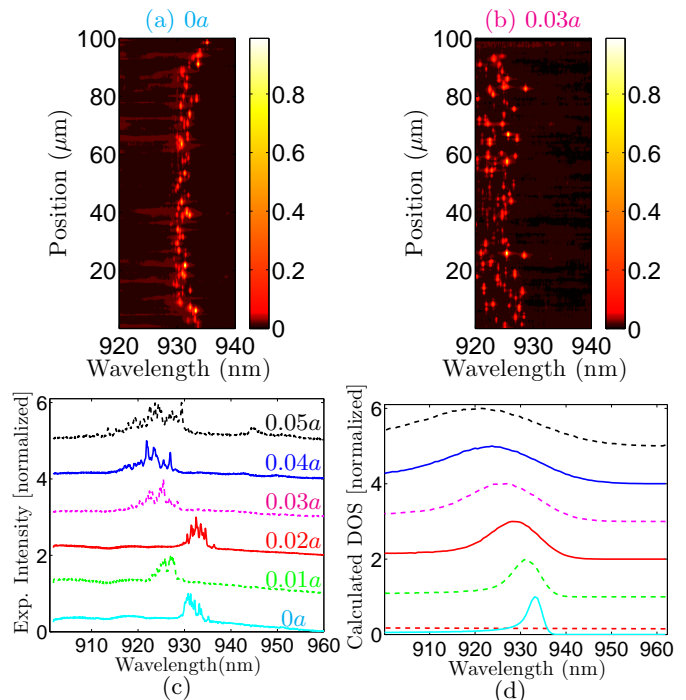


FIG. 3. (a,b) Experimental normalized intensity spectra obtained by scanning along the waveguide position for two different amounts of extrinsic disorder as indicated in the figure. (c) Experimental spatially-integrated intensity for varying degrees of extrinsic disorder as labelled in the figure. (d) Calculated ensemble averaged DOS (normalized) for the fundamental waveguide mode for the six disordered samples in (c). The red-dashed line in the lowest disorder case is given by $A \frac{\lambda_{\min}^2}{\lambda^2}$ with $A = 0.2$ and represents the qualitative contribution of radiation modes to the DOS. The amount of intrinsic disorder in all samples is $\sigma_i = 0.005a$ (1.2 nm).

V. NUMERICALLY COMPUTED DISORDERED INSTANCES FROM A FINITE-SIZE PCW

Having identified the limits of perturbation theory above, we now present some brute force calculations of the LDOS using full 3D FDTD computations in a disordered PCW lattice. The numerical complexity is very demanding so we are restricted to much smaller waveguide lengths than used in the experiment; also, we can only compute a small number of instances which are not enough to compute the ensemble average trend shown in Fig. 3. This is mainly due to the large memory requirements of the simulation volume since it cannot be reduced by using symmetric boundary conditions due to symmetry breaking caused by disorder. Nevertheless, such calculations are useful for getting a physical picture of what is happening for a particular instance and section of a disordered PCW.

To show that the DOS varies from instance to instance given the disorder is kept fixed, we calculate the projected LDOS $\rho_\mu(\mathbf{r}, \omega)$ for ten statistically disordered

finite-length PCWs, as shown in Fig. 4, by directly computing the numerically exact photonic Green function of the PCW (see Ref. 6 for numerical implementation details) using the 3D FDTD method [46]. The samples we simulate are only $7.2 \mu\text{m}$ long (30 unit cells). With the waveguide cross section in the xy plane, denoting the waveguide direction as x and the origin at the centre of the waveguide, we compute the LDOS of a y -oriented dipole $\rho_y(0, \omega)$ placed at the anti-node of e_y , which occurs at the origin. The intrinsic/extrinsic disorder values are $0.005a(1.2 \text{ nm})$, $0.02a(4.8 \text{ nm})$, respectively. While ten instances which are only 30 unit cells long are not enough to conclude the existence of a mean blueshift of the mode-edge, the variance in LDOS profiles can partially explain the discrepancy observed in Fig. 3(b) for $\sigma_e = 0.02a(4.8 \text{ nm})$. For completeness, Fig. 4 also shows examples of disorder induced localized modes that appear both above and below the mode edge. These modes are formed via multiple scattering in cavity-like defects introduced via disorder.

We highlight that we have found a 2D FDTD method to be inadequate for computing the Green function and LDOS for the PCW slab. Firstly, the mode edge for a 2D PCW with the same structural parameters (apart from the slab height) is different ($1.2 \mu\text{m}$) and secondly, a 2D PCW does not possess radiation or leaky modes and out-of-plane decay cannot be computed. Hence the computed Green function does not accurately capture the realistic 3D resonance shifts expected in the LDOS. Although a 2D calculation can capture the qualitative modal profile of the localized modes, their sensitivity to disorder is quite different to 3D quasimodes. Thus one requires a 3D FDTD model to compute the LDOS for a PCW slab in general.

VI. DISCUSSION AND CONNECTIONS TO PREVIOUS WORKS

Our theory, though perturbative, provides an intuitive and computationally efficient semi-analytical approach to producing experimentally relevant results for moderate amounts of extrinsic disorder and provides upper bounds for high amount of extrinsic disorder. One computation which includes computing the ideal Bloch modes, Monte Carlo runs for the expectations and Riemann integrals for a given amount of disorder takes roughly 3 hours on a single-core CPU whereas computing the LDOS of a $7.2 \mu\text{m}$ long disordered PCW using 3D FDTD takes approximately 10 CPU hours for *each* disorder instance on a cluster using 20 multi-core CPU nodes.

As we have stated before, the bump-perturbation polarization model is crucial to our findings. It is not the exact shape of the bump that is important (see Refs. [29, 32]) but the use of asymmetric polarizabilities that yields a non-zero net mean frequency shift. In the context of disorder-induced losses where all three polarization models produce similar results, previously we

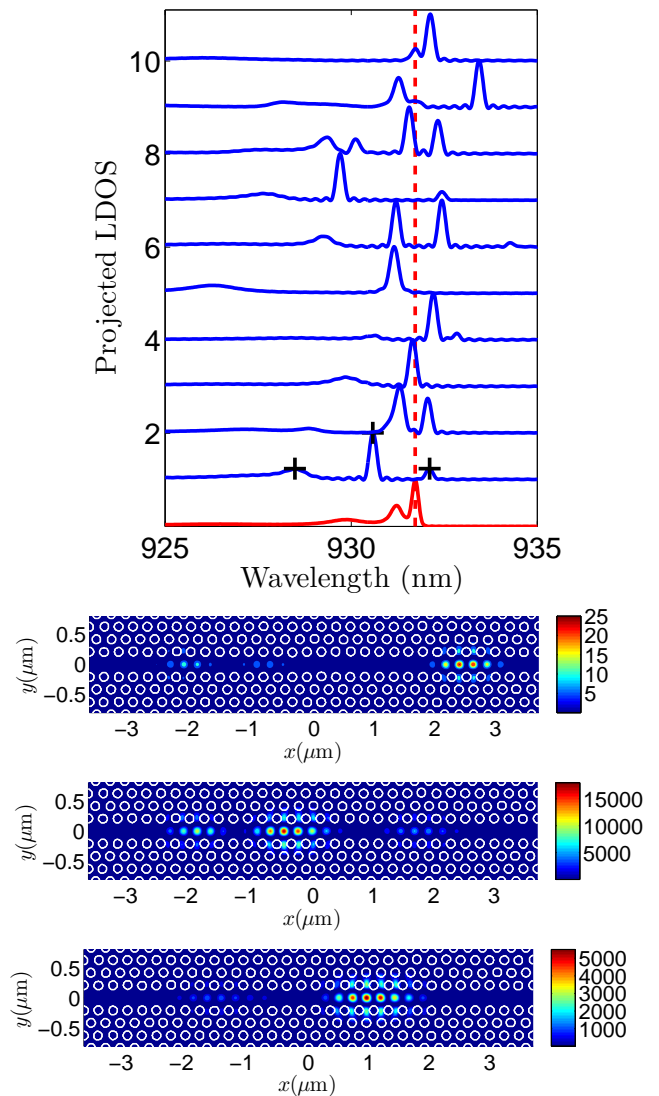


FIG. 4. (Colour online) (Top) Projected LDOS values of a y -oriented dipole centred at the anti-node of e_y , computed for ten instances of disorder (blue/dark-solid) with internal/external disorder values of $\sigma_i = 0.005a(1.2 \text{ nm})$, $\sigma_e = 0.02a(4.8 \text{ nm})$ respectively. For reference, the LDOS with no *extrinsic* disorder (red/light-solid) and ideal mode edge (dashed-red/light vertical line) are also shown. All LDOS instances are normalized to their own LDOS peak. The length of the waveguides was kept fixed at $7.2 \mu\text{m}$ (30 unit cells). (Bottom) As highlighted by the black markers (+) on the Projected LDOS instance, starting from above (right) and going below (left) the mode-edge, localized mode intensity of $|e_y|^2$ is shown.

have argued that the bump polarization model should be best suited for modelling disorder characterized via rapid radial fluctuations and the smooth-perturbation model should be valid as long as the air-slab interface remains nearly circular [30] which is indeed the case considered in this work. To resolve this ambiguity, we rely on the comparison with experimental findings (see Sec. IV) which

indicates that the bump-polarization model (in the absence of any other models in the literature) is best suited for all types of disorder and various disorder-induced phenomena in PCWs.

Reference 30 highlighted the importance of accounting for local field effects in PCWs by computing disorder-induced resonance shifts for the three polarization models mentioned in Sec. II. While the impact of disorder on the DOS is qualitatively well known, to our knowledge, no one has quantified the expected resonance shifts or spectral broadening as a function of disorder and computed the disordered DOS which is found in good qualitative agreement with experiments. Previously, spectral broadening of the bandstructure was observed experimentally by Le Thomas *et al.* [47] and predicted theoretically by Savona [31] whose findings showed increased spectral broadening of the bandstructure as the disorder increases, but did not predict a blueshift or quantify the expected shift or broadening as a function of disorder.

VII. CONCLUSIONS

Through theory and experiment, we have shown that accurate modelling of local field effects is critical for computing experimentally relevant mean frequency shifts and realistic DOS profiles in PCWs. These findings also point

out the possible limitations of disorder polarization models that do not include local field effects or include local field effects through the use of symmetric polarizabilities. For moderate amounts of disorder, our computationally efficient semi-analytical perturbative approach yields results that are in good qualitative agreement with experiments and can be used to compute realistic quantities such as Purcell factor enhancements in PCWs with embedded quantum dots. We have also shown examples of the numerically exact LDOS for various disordered instances and the underlying disordered-induced resonance modes on a small PCW using a rigorous 3D FDTD approach. Future work will focus on developing a non-perturbative approach that takes into account multiple scattering to better model high amounts of disorder.

ACKNOWLEDGMENTS

This work was supported by the National Science and Engineering Research Council of Canada and Queen's University, Canada. Alisa Javadi, P.D. García and Peter Lodahl gratefully acknowledge the financial support from the Danish Council For Independent Research (Natural Sciences and Technology and Production Sciences), The Villum Foundation, and the European Research Council (ERC consolidator Grant "ALLQUANTUM").

-
- [1] T. F. Krauss, *Nat. Photonics* **2**, 448 (2008).
 - [2] P. Lodahl, S. Mahmoodian, and Stobbe, Søren, (2013), [arXiv:1312.1079](https://arxiv.org/abs/1312.1079).
 - [3] T. Yoshie, A. Scherer, J. Hendrickson, G. Khitrova, H. M. Gibbs, G. Rupper, C. Ell, O. B. Shchekin, and D. G. Deppe, *Nature* **432**, 200 (2004).
 - [4] K. Hennessy, A. Badolato, M. Winger, D. Gerace, M. Atatüre, S. Gulde, S. Fält, E. L. Hu, and A. Imamoglu, *Nature* **445**, 896 (2007).
 - [5] T. Lund-Hansen, S. Stobbe, B. Julsgaard, H. Thyrrestrup, T. Sünner, M. Kamp, A. Forchel, and P. Lodahl, *Phys. Rev. Lett.* **101**, 113903 (2008).
 - [6] P. Yao, V. Manga Rao, and S. Hughes, *Laser Photon. Rev.* **4**, 499 (2010).
 - [7] A. Laucht, S. Pütz, T. Günthner, N. Hauke, R. Saive, S. Frédérick, M. Bichler, M.-C. Amann, A. Holleitner, M. Kaniber, and J. Finley, *Phys. Rev. X* **2**, 011014 (2012).
 - [8] P. Colman, C. Husko, S. Combrié, I. Sagnes, C. W. Wong, and A. De Rossi, *Nat. Photonics* **4**, 862 (2010).
 - [9] C. Monat, M. Spurny, C. Grillet, L. O'Faolain, T. F. Krauss, B. J. Eggleton, D. Bulla, S. Madden, and B. Luther-Davies, *Opt. Lett.* **36**, 2818 (2011).
 - [10] J. Li, L. O'Faolain, and T. F. Krauss, *Opt. Express* **20**, 17474 (2012).
 - [11] N. Skivesen, A. Têtù, M. Kristensen, J. Kjems, L. H. Frandsen, and P. I. Borel, *Opt. Express* **15**, 3169 (2007).
 - [12] J. Topol'ancik, P. Bhattacharya, J. Sabarinathan, and P.-C. Yu, *Appl. Phys. Lett.* **82**, 1143 (2003).
 - [13] T. Baba, *Nat. Photonics* **2**, 465 (2008).
 - [14] S. Hughes, L. Ramunno, J. Young, and J. Sipe, *Phys. Rev. Lett.* **94**, 033903 (2005).
 - [15] D. Gerace and L. C. Andreani, *Opt. Lett.* **29**, 1897 (2004).
 - [16] B. Wang, S. Mazoyer, J. Hugonin, and P. Lalanne, *Phys. Rev. B* **78**, 245108 (2008).
 - [17] W. Song, R. A. Integlia, and W. Jiang, *Phys. Rev. B* **82**, 235306 (2010).
 - [18] L. O'Faolain, T. P. White, D. O'Brien, X. Yuan, M. D. Settle, and T. F. Krauss, *Opt. Express* **15**, 13129 (2007).
 - [19] F. Wang, J. S. Jensen, and O. Sigmund, *Photonics Nanostructures - Fundam. Appl.* **10**, 378 (2012).
 - [20] N. Mann, S. Combrié, and P. Colman, *Opt. Lett.* **38**, 4244 (2013).
 - [21] L. O'Faolain, S. Schulz, D. M. Beggs, T. P. White, M. Spasenović, L. Kuipers, F. Morichetti, A. Melloni, S. Mazoyer, J. P. Hugonin, P. Lalanne, and T. F. Krauss, *Opt. Express* **18**, 27627 (2010).
 - [22] J. Sancho, J. Bourderionnet, J. Lloret, S. Combrié, I. Gasulla, S. Xavier, S. Sales, P. Colman, G. Lehoucq, D. Dolfi, J. Capmany, and A. De Rossi, *Nat. Commun.* **3**, 1075 (2012).
 - [23] S. John, *Phys. Rev. Lett.* **58**, 2486 (1987).
 - [24] J. Topolancik, B. Ilic, and F. Vollmer, *Phys. Rev. Lett.* **99**, 253901 (2007).
 - [25] M. Patterson, S. Hughes, and S. Combrié, *Phys. Rev. ...* **102**, 253903 (2009).
 - [26] L. Sapienza, H. Thyrrestrup, S. r. Stobbe, P. D. Garcia, S. Smolka, and P. Lodahl, *Science* **327**, 1352 (2010).

- [27] H. Thyrrstrup, S. Smolka, L. Sapienza, and P. Lodahl, *Phys. Rev. Lett.* **108**, 113901 (2012).
- [28] J. Liu, P. D. Garcia, S. Ek, N. Gregersen, T. Suhr, M. Schubert, Mørk, J, S. Stobbe, and P. Lodahl, *Nat. Nanotechnol.* **9**, 285 (2014).
- [29] L. Ramunno and S. Hughes, *Phys. Rev. B* **79** (2009), 10.1103/PhysRevB.79.161303.
- [30] M. Patterson and S. Hughes, *Phys. Rev. B* **81**, 245321 (2010).
- [31] V. Savona, *Phys. Rev. B* **83**, 85301 (2011).
- [32] S. Johnson, M. L. Povinelli, M. Soljačić, A. Karalis, S. Jacobs, and J. D. Joannopoulos, *Appl. Phys. B* **81**, 283 (2005).
- [33] A. Javadi, S. Maibom, L. Sapienza, H. Thyrrstrup, P. D. García, and P. Lodahl, *Opt. Express* **22**, 30992 (2014).
- [34] S. Johnson, M. Ibanescu, M. Skorobogatiy, O. Weisberg, J. Joannopoulos, and Y. Fink, *Phys. Rev. E* **65**, 066611 (2002).
- [35] D. Marcuse, *Theory of Dielectric Optical Waveguides*, 1st ed. (Academic Press, New York, 1974) pp. 101–102.
- [36] L. C. Andreani and D. Gerace, *Phys. status solidi* **244**, 3528 (2007).
- [37] J. D. Jackson, *Am. J. Phys.*, 3rd ed., Vol. 67 (John Wiley & Sons, 1999) p. 841.
- [38] P. D. Garcia, A. Javadi, H. Thyrrstrup, and P. Lodahl, *Appl. Phys. Lett.* **102**, 031101 (2013).
- [39] D. Fussell, S. Hughes, and M. Dignam, *Phys. Rev. B* **78**, 1 (2008).
- [40] V. Rao and S. Hughes, *Phys. Rev. B* **75**, 205437 (2007).
- [41] P. Yao and S. Hughes, *Phys. Rev. B* **80**, 165128 (2009).
- [42] P. Kristensen and S. Hughes, *ACS Photonics* **1**, 2 (2013).
- [43] K. M. Lee, P. T. Leung, and K. M. Pang, *J. Opt. Soc. Am. B* **16**, 1409 (1999).
- [44] R. C. Ge, P. Kristensen, J. F. Young, and S. Hughes, *New J. Phys.* **16**, 113048 (2014).
- [45] M. Patterson, S. Hughes, S. Schulz, and D. Beggs, *Phys. Rev. B* **80**, 195305 (2009).
- [46] “Lumerical Solutions Inc.” .
- [47] N. Le Thomas, H. Zhang, J. Jágerská, V. Zabelin, R. Houdré, I. Sagnes, and A. Talneau, *Phys. Rev. B* **80**, 125332 (2009).